



HAL
open science

Indirect nanoscale characterization of polymer photoresist wetting using ultra-high frequency acoustic waves

Abbas Salhab, Julien Carlier, Malika Toubal, David Troadec, Philippe Garnier, Thomas Mercadier, Pierre Campistron, Vincent Thomy

► To cite this version:

Abbas Salhab, Julien Carlier, Malika Toubal, David Troadec, Philippe Garnier, et al.. Indirect nanoscale characterization of polymer photoresist wetting using ultra-high frequency acoustic waves. *Physica Scripta*, 2023, 98 (10), pp.105967. 10.1088/1402-4896/acfa45 . hal-04211683

HAL Id: hal-04211683

<https://hal.science/hal-04211683>

Submitted on 19 Sep 2023

HAL is a multi-disciplinary open access archive for the deposit and dissemination of scientific research documents, whether they are published or not. The documents may come from teaching and research institutions in France or abroad, or from public or private research centers.

L'archive ouverte pluridisciplinaire **HAL**, est destinée au dépôt et à la diffusion de documents scientifiques de niveau recherche, publiés ou non, émanant des établissements d'enseignement et de recherche français ou étrangers, des laboratoires publics ou privés.

Indirect nanoscale characterization of polymer photoresist wetting using ultra-high frequency acoustic waves

A. Salhab¹, J. Carlier¹, M. Toubal¹, D. Troadec¹, P. Garnier², T. Mercadier², P. Campistron¹ and V. Thomy¹

¹Univ. Polytechnique Hauts-de-France, Univ. Lille, CNRS, Centrale Lille, UMR 8520 - IEMN- Institut d'Electronique de Microélectronique et de Nanotechnologie, F-59000 Lille, France

²STMicroelectronics, 850 rue Monnet, F-38926 Crolles, France

Email: Abbas.Salhab@uphf.fr; Julien.Carlier@uphf.fr

Received xxxxxx

Accepted for publication xxxxxx

Published xxxxxx

Abstract

The wetting of surfaces with patterns in the order of a hundred nanometers is often a complex phenomenon to analyze and control. In the semiconductor industry, whether it is during the surface cleaning steps or the deposition of the protective mask (photosensitive liquid resin that is then cross-linked), the conformity of the deposit of the liquid layer on the patterned surface must be perfect or else the functionality of the targeted electronic component will be compromised. Thus, understanding the surface wetting of these liquids allows the implementation of optimized processes. In this paper, we present a method of indirect wetting characterization of a photoresist based on ultra-high frequency (# GHz) acoustic waves. This resin is a commercial product called GKR 4602 (belonging to the KrF series of positive photoresists), which is coated in two different ways: either directly onto the surface of a patterned silicon wafer, or after application of a solvent, Propylene Glycol Ethyl Ether (PGEE), which then acts as a pre-wetting layer. The patterned wafer, playing the role of electrical insulation (Deep Trench Isolation, DTI) are 200 nm wide, deep trenches with a high aspect ratio (> 50). The originality of this paper lies in the validation of the acoustic characterization by direct observation of the wetting of the cross-linked resin. To do so, we used a FIB (Focused Ion Beam) microscope which allowed us to make cuts and capture localized images of the wetting state of the photoresist. Moreover, all the results obtained (resins and patterned silicon surfaces) are directly from the microelectronics industry (STMicroelectronics), showing that our method is fully compatible with an industrial approach.

Keywords: Acoustics, Deep trench isolation, Micro and Nano-technology, Micro-electromechanical systems, Semiconductors, Surface wetting, Wetting, Focus Ion Beam

1. Introduction

In the semiconductor industry, the manufacturing of microchips consists of many processes, reaching up to hundreds [1]. Most of the industries carry out the processes in an "ISO class 1" cleanroom [2]. Despite the measures to clean

the Si surface, contaminants may still come from the different processes included in the microchip fabrication. About one third of the manufacturing processes are related to surface treatments and decontamination of particles. Thus, wet processes are necessary for cleaning and surface preparation before and after each process [3]. For example, Chemical Mechanical Planarization (CMP) [4], is used to flatten silicon wafers and remove surface topologies by utilizing nano-sized abrasive particles in a slurry mixture. This operation could result in contamination across the wafer's surface. In addition, processes like lithography, dry and wet etching, and metal layer deposition require a post-cleaning process to remove the inherent contaminants [5].

For instance, before the etching process, a mask (usually a photoresist polymer) is used to protect the desired area [6][7]. The presence of organic contaminants on the surface can inhibit the adherence of the photoresist film to the wafer's surface.

While the sizes of electronic components are decreasing drastically to a few hundred nanometers (following Moore's law), this problem of removing contaminations becomes crucial [8]. One typical silicon structure is trench with a high aspect ratio that plays the role of electrical insulation. In both of these cases, the basic problem is to ensure that the wetting of the cleaning or etching fluid or the liquid polymer contacts the entire surface, including structures with large aspect ratios and typical dimensions in the order of a hundred nanometers [9]–[10].

Different techniques exist in the literature to characterize the wetting efficiency of liquids inside micro-nanopatterned surfaces, such as ATR-FTIR (Attenuated Total Reflectance-FTIR) [11], and EIS (Electrochemical Impedance Spectroscopy) [12], which enable real-time monitoring of the wetting phenomenon of the liquid [13][15].

For our part, we have developed an acoustic characterization method based on ultra-high frequency (up to 5 GHz) [16][17] that uses bulk acoustic waves to characterize the wetting efficiency of a liquid droplet deposited on micro-nanopatterned silicon surfaces.

However, all these techniques suffer from the same drawback. The validation of the results they allow to be obtained cannot be done optically under the same conditions, i.e., in real time and at very small scales. To meet this

necessary validation, a lot of groups have attempted to combine the characterization of wetting on textured surfaces at micro- or even nanometric scales with direct observation by scanning electron microscope or other technologies. The Varanasi pioneering group thus frozen a drop of water and then made a cut using an FIB in order to observe the triple line and even under the drop by SEM [18]. We also used polymerized polymer drops on the surface to observe the deformation of the triple line [19]. In this letter, we propose to combine the two techniques of polymer use and FIB cutting. This allows us to visualize the behavior of polymerized polymer films, which is the image of their wetting on surfaces with trenches a hundred nanometers wide and with high aspect ratios.

In the first part of this paper, we will present an application of the acoustic method to characterize the wetting over a Deep Trench Isolation (DTI) [20][21] patterned silicon wafer using a commercial photoresist named GKR 4602 that is used as a mask during the etching processes at STMicroelectronics. Then we will study the impact of using an additional solvent layer of Propylene Glycol Ethyl Ether (PGEE) as a pre-wetting layer. This solvent layer will be dispensed before GKR 4602, in order to improve the wetting efficiency. In the second part, we will use FIB imaging of a cross-sectional cut inside the DTI patterned wafer sample. Thus, it will be possible to visualize the filling of this photoresist inside the DTI features and finally compare the images to the results obtained with the acoustic characterization method.

2. Experimental setup

2.1. DTI geometry

The DTI wafers are composed of an etched network of trenches (Figure 1(a)) inside periodic structures called matrices (see figure S1 in supplementary material). The trenches are 200 nm in width and 10 μm in depth, and they are etched on the front side of a 300 mm wafer that is 775 ± 10 μm thick and fabricated by STMicroelectronics. On the front side of the wafer, we find three layers composed of 7.5 nm silicon dioxide (SiO_2), 55 nm silicon nitride (Si_3N_4), and 80 ± 20 nm (SiO_2), respectively, stacked as shown in Figure 1(b).

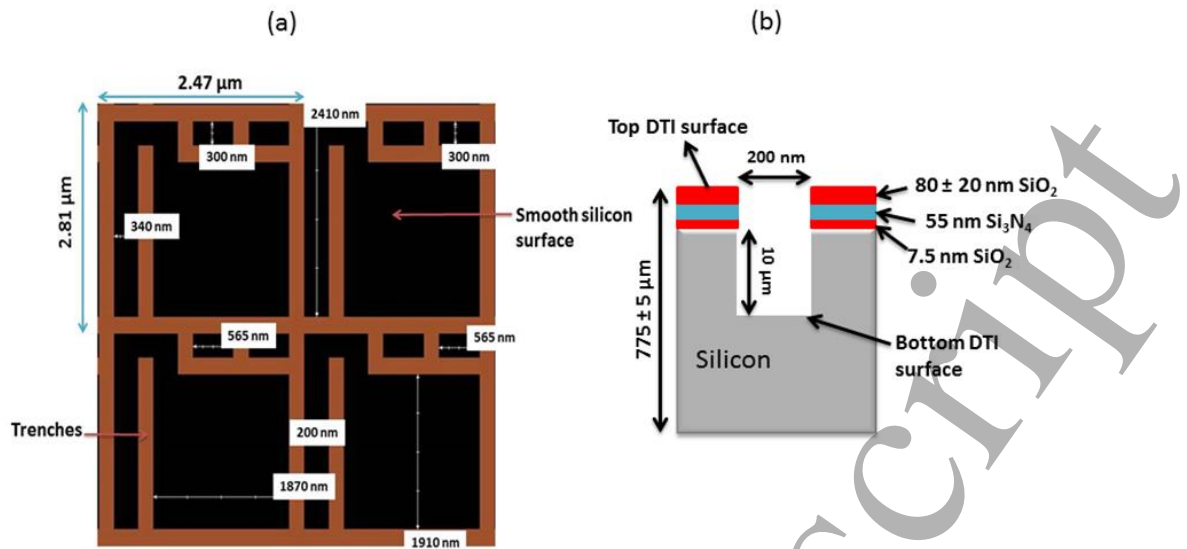


Figure 1. (a) Image of the DTI network where the brown color represents the etched trenches and the black colors represent the Si pillars; (b) Schematic of an etched trench.

2.2. Characterization by acoustic reflectometry

The wetting characterization using acoustic reflectometry is developed at the IEMN laboratory. It consists of measuring the reflection coefficient in the time domain of ultra-high frequency longitudinal waves generated by piezoelectric transducers built on the backside of a $7 \times 7 \text{ cm}^2$ DTI silicon wafer.

The piezoelectric transducers are composed of thin metallic layers: 10 nm titanium “Ti” + 50 nm platinum “Pt” + 500 nm Zinc Oxide “ZnO” + 50 nm Pt deposited consecutively in the same order they appear. The Zinc Oxide (ZnO) layer is sandwiched between a ground electrode, composed of titanium (Ti) and platinum (Pt), and another platinum counter electrode. The thicknesses of the various materials have been simulated in order to reach a resonance at a desired frequency with a maximum of the signal at the receiving end [22]. For the given thickness of 500 nm of ZnO and a diameter of 100 μm of the counter electrode, obtained by a photolithography process, we get a central frequency of 3.5 GHz in the longitudinal mode.

The acoustic reflectometry method is shown in Figure 2. The longitudinal waves will be first reflected back from the bottom of the trenches, then from the top. This will result in two main echoes, A_1 and A_2 , respectively. In our study, we are mainly concerned with the A_1 echo, which is an indicator of the wetting inside the trenches. The measurement is carried out by first acquiring the scattering parameter $S_{11}(f)$ (complex reflected/incident voltage ratio) using a SussMicrotech probe coupled with a Rhode & Schwarz 300 kHz to 8 GHz Vector Network Analyzer (VNA) shown in Figure 3. The general expression of $S_{11}(f)$ is given in equation (1). $S_{11}^{el}(f)$ and

$S_{11}^{ac}(f)$ correspond to the purely electrical and purely acoustic responses of the transducer. K corresponds to the electro-acousto-electrical conversion coefficient [23]. Applying an inverse Fourier transform to $S_{11}(f)$, the amplitudes of the reflected echoes on the bottom and the top of the structures (A_1 and A_2) are obtained in the time domain $S_{11}(t)$ (Equation (2)). The calculation of the acoustic reflection coefficient is not possible directly due to the fact that the value of K is unknown [22]. Thus, an indirect method consists of normalizing the amplitude obtained in the presence of liquid with the equivalent amplitude obtained when the wafer is exposed to air in order to obtain the acoustic reflection coefficient. The reflection coefficient on the bottom surface of the DTI (r_1) is given in equation (3).

$$S_{11}(f) = S_{11}^{el}(f) + KS_{11}^{ac}(f) \quad (1)$$

$$S_{11}(t) = F^{-1}[S_{11}^{el}(f)] + F^{-1}[KS_{11}^{ac}(f)] \quad (2)$$

$$|r_1| = \frac{A_1^{Charge}}{A_1^{Air}} \quad (3)$$

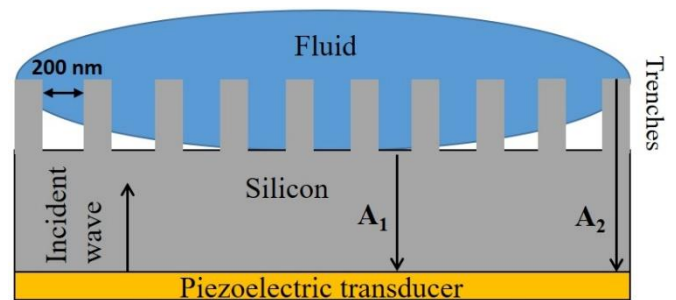


Figure 2. Schematic of the wetting characterization using the acoustic reflectometry method.

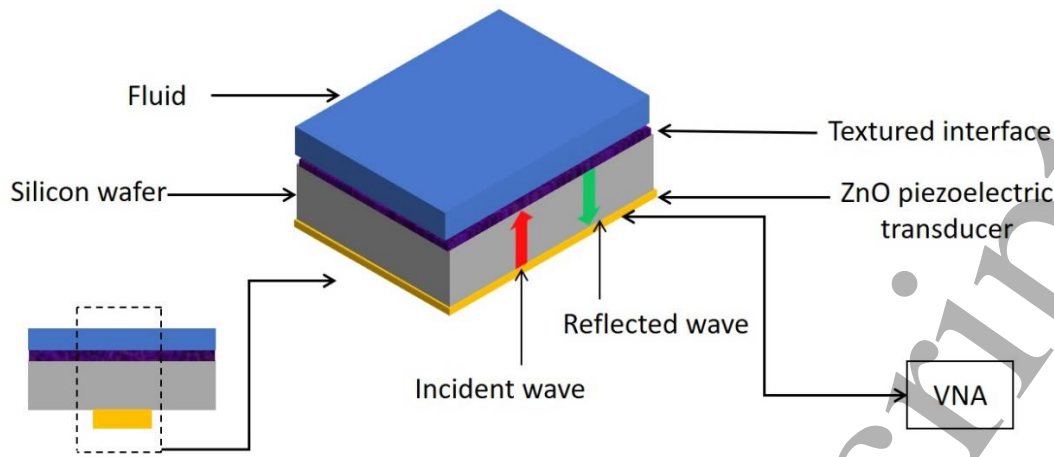


Figure 3. Schematic of the acoustic measurement bench for the characterization of textured surface .

It is to be noted that the signal received by the transducer and then acquired by the instrumentation is, at a given time, a spatially mean value of the signal coming from the surface ($100\ \mu\text{m}$ disk diameter) located at the vertical position of the transducer. The sensitivity of the acoustic method depends mainly on two factors: the high contrast between air and fluid acoustic impedances [24] and the frequency of the transducer [16]. The acoustic impedance Z of a material is given as a function of the density ρ and the acoustic wave propagation velocity c in the material ($Z = \rho c$).

On the DTI patterned wafer sample, the photoresist is coated by spin coating (using RC8 Karl Süss equipment) in two closed cycles according to the following parameters: Rotational velocity $V_1 = 3650$ r.p.m., time $t_1 = 40$ s, and acceleration $A_1 = 1000$ r.p.m./s; $V_2 = 1500$ r.p.m., $t_2 = 30$ s, and $A_2 = 1000$ r.p.m./s. The indicated rotational velocity (V_1) will result in a $3.5\ \mu\text{m}$ thick photoresist layer. The photoresist has a density $\rho_1 = 1015\ \text{kg}\cdot\text{m}^{-3}$ and a kinematic viscosity $\nu_1 = 124 \times 10^{-6}\ \text{m}^2\cdot\text{s}^{-1}$. After the photoresist deposition, the sample is baked at 130°C for 90 s.

The PGEE solvent ($\rho_2 = 897\ \text{kg}\cdot\text{m}^{-3}$, $\nu_2 = 2.47 \times 10^{-6}\ \text{m}^2\cdot\text{s}^{-1}$, surface tension $\gamma = 26.5\ \text{mN}\cdot\text{m}^{-1}$), corresponding to the pre-wetting layer, is dispensed according to the following parameters: $V_3 = 1500$ r.p.m., $t_3 = 2$ s, and $A_3 = 1000$ r.p.m./s, and GKR 4602 afterwards.

As a first step, the reference reflection coefficient ($r_{Si/GKR4602}$) at the interface between the silicon and the GKR 4602 layer needs to be measured. For that purpose, a 3-inch smooth Si wafer of, $380 \pm 20\ \mu\text{m}$ in thickness is coated with a photoresist according to the following parameters: $V_4 = 1000$ r.p.m., $t_4 = 90$ s, and $A_4 = 1000$ r.p.m./s. The indicated

rotational velocity (V_4) will result in a $6.5\ \mu\text{m}$ thick photoresist layer. After the photoresist deposition, the sample is baked at 130°C for 90 s. Here, the coating of the photoresist is carried out at a lower rotational velocity to obtain a thicker layer that will enable a good separation of the echoes at the interface between the Si and the photoresist.

3. Results and discussions

3.1. Acoustic characterization

To measure $r_{Si/GKR4602}$, the reflection coefficient at the silicon and GKR 4602 interface, the photoresist is coated on the smooth Si wafer. The echoes diagram is shown in Figure 4. The measurements are performed with a transducer over a bandwidth of [1–6 GHz]. The reference to air (solid line) corresponds to only one echo occurring at 89.04 ns. The echoes diagram corresponding to the photoresist coated on the silicon wafer (dotted line) shows a first echo occurring at 89.04 ns at the same time as the echo relative to air. The reflection coefficient at the silicon/GKR 4602 interface is then deduced to be: $r_{Si/GKR4602} = 0.72$.

The other echoes correspond to the multiple reflections inside the photoresist.

After obtaining the reference value $r_{Si/GKR4602}$, the next step is to characterize the interface between the photoresist and the DTI patterned wafer, knowing that this interface is an indirect view of the polymer wetting on this surface prior to its reticulation. For that purpose, we use two identical DTI patterned wafer samples. On the first one (sample 1), only the

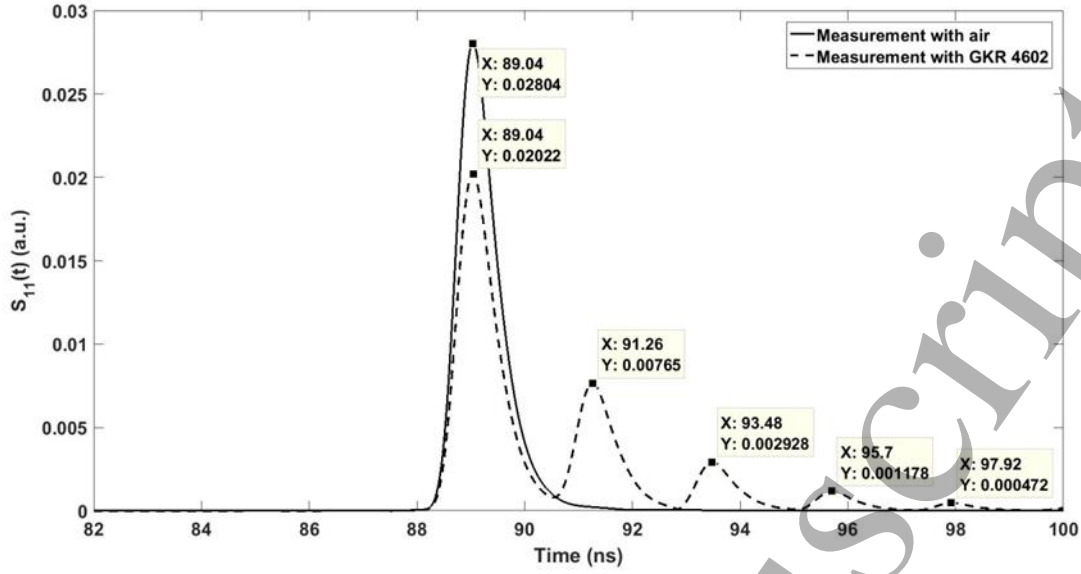


Figure 4. Echoes diagram ($S_{11}(t)$) at air (solid line) and at coated GKR 4602 (dotted line) for a transducer (found on the smooth surface wafer sample) of a central frequency equal to 3.5 GHz taken on a bandwidth of [1–6 GHz].

photoresist is coated. On the second sample (sample 2), a pre-wetting layer of PGEE is first coated, followed by a layer of photoresist.

The echoes diagrams taken with transducers T_3 and T_4 found on samples 1 and 2, respectively, are shown in Figure 5. We notice that for both measurements (with air and with photoresist), different echoes can be seen, knowing that the first of them, which occurs at $t_2 = 181.4$ ns, is of interest. It represents the reflection of the incident waves on the bottom surface of the trenches. The following echoes that arrive afterwards depict reflections of the incident wave on the walls and on the top surface of the trenches. It is interesting to note that the echoes that follow the first one are remarkably damped compared to the same echoes obtained from the air measurement. This indicates the transfer of the acoustic energy to the photoresist layer present inside the trenches. To indirectly quantify the wetting of the photoresist on the DTI, the wet bottom area “ S_w ” is calculated, which quantifies the surface area of the wet bottom area [17]. If part of the lower surface of the trenches is covered by photoresist and the rest of the bottom surface is filled by air, the reflection coefficient r_l is then given as follows:

$$r_l = S_w r_{Si/GKR4602} + (1 - S_w) r_{Si/air} \quad (4)$$

$r_{Si/air} = 1$, since there is no transfer of acoustic energy when the medium at the interface is air [25]. Thus, S_w is calculated as:

$$S_w = \frac{r_{Si/air} - r_l}{r_{Si/air} - r_{Si/GKR4602}} \quad (5)$$

A series of 5–6 measurements on each sample, over various DTI matrices, have been undertaken.

Each measurement of r_l is taken over a circular transducer of 100 μm in diameter. Thus, each measurement is an evaluation of local wetting over a surface area of 7854 μm^2 . Using the dimensions in Figure 1(a), the trenches represent about 39.2% of the patterned surface. Therefore, each measurement is an assessment of the total fill over 3078.77 μm^2 of trench bottom surface area.

Table 1 represents the summary of the measurements on the two samples (with and without the pre-wetting layer) with 5–6 different transducers. The transducers were chosen close to the center of the wafer (area relative to a circle of 4 cm in diameter) to ensure the best photoresist film uniformity during spin coating.

Table 1. Summary of the acoustic measurements obtained using different transducers found on the two DTI patterned samples.

Transducer	Sample 1		Sample 2	
	r_l	S_w (%)	r_l	S_w (%)
T ₁	0.78	78.6	0.75	89.3
T ₂	0.77	82.1	0.74	92.9
T ₃	0.84	57.1	0.73	96.4
T ₄	0.83	60.7	0.72	100
T ₅	0.79	75	0.77	82.8
T ₆	0.76	85.7	-	-

The average (\bar{S}) and the standard deviation ($\bar{\sigma}$) of wetted surface percentage S_w are found to be: $\bar{S}_1 = 73.2\%$, $\bar{\sigma}_1 = 10.7$ for sample 1 and $\bar{S}_2 = 92.3\%$, $\bar{\sigma}_2 = 5.9$ for sample 2.

We come to the clear conclusion that sample 2, with the added pre-wetting layer, shows a higher wetted surface percentage of photoresist inside the trenches compared to

sample 1 ($\bar{S}_2 > \bar{S}_1$). In addition, this pretreatment seems to improve the filling uniformity inside the trenches ($\bar{\sigma}_2 < \bar{\sigma}_1$).

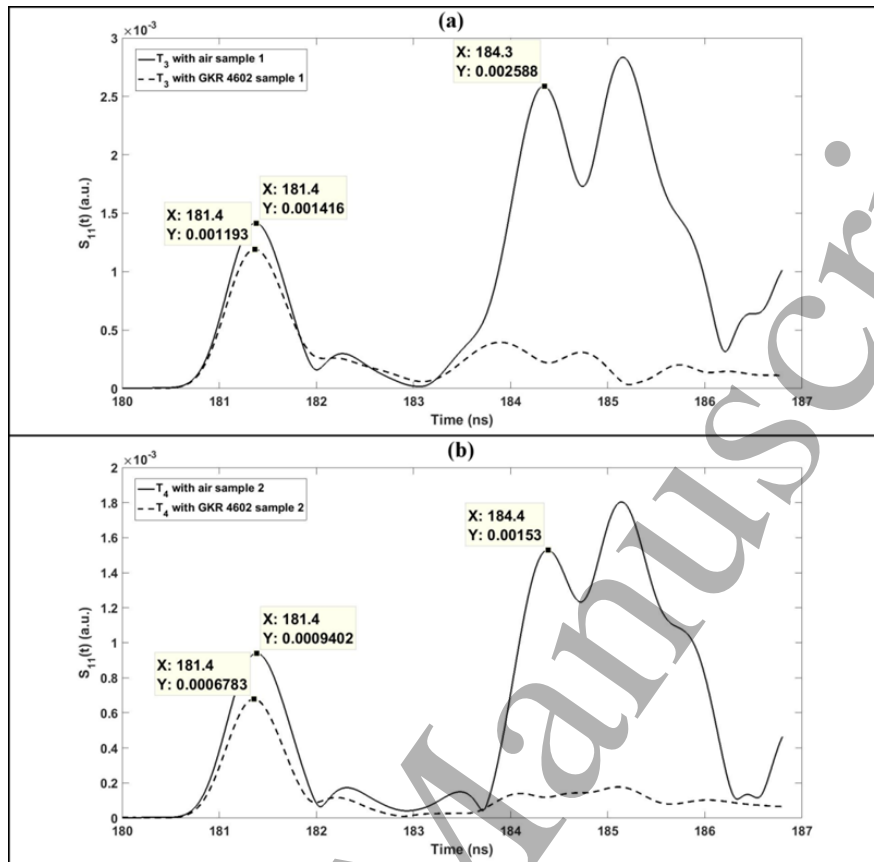


Figure 5. Echoes diagram ($S_{11}(t)$) at air (solid line) and at coated GKR 4602 (dotted line) for (a) Transducer T3 located at DTI sample 1; (b) Transducer T4 located at DTI sample 2.

In order to consolidate our results, images of the filling of the trenches were set up using FIB-SEM (Focused Ion Beam-Scanning Electron Microscope) imagery. The FIB-SEM images comparing the filling state of the trenches with and without the pre-wetting layer are presented next.

3.2. FIB imagery

The advantage of using FIB-SEM is that it can reveal subsurface structural details, by making precise cuts with accelerated ions and then imaging the exposed surface with a high-resolution SEM.

To this end, we use two new samples, 3 and 4. On Sample 3 only the photoresist layer is coated, while on sample 4, the pre-wetting and photoresist layers are coated.

Figure 6 presents the SEM image of a DTI matrix of sample 3 (photoresist coated without the pre-wetting layer). Looking at Figure 6(a), we note that there is no presence of photoresist on the bottom surface of trenches 1,3,5,7, and 9 (counting from the left) and that the rest of the trenches show the

presence of the photoresist at the bottom with large air bubbles inside. In Figure 6(b), the 9th trench (from the left) has multiple small air bubbles (small black holes), while the 6th, 8th, and 12th trenches have relatively larger air gaps, with the bottom of the trenches filled by the photoresist. The rest of the trenches (Figure 6(b)) appear to be completely filled. In conclusion, the FIB images of sample 3 (without a pre-wetting layer) show that the bottom wetting is not homogeneous. Several places on the bottom surface of some trenches are not filled with photoresist. This non-uniformity is consistent with the acoustic characterization. Indeed, looking at the FIB cut made on sample 3, we notice that out of the 36 trenches shown (see figure S2 in supplementary material), only 29 show the presence of photoresist on the bottom surface, indicating a wetting percentage of 80.6%.

Figure 7 shows the SEM images corresponding to the DTI matrix of sample 4. The gray color inside the trenches represents the photoresist, while the black one represents the wetting defect (or trapped air bubbles). These trapped air

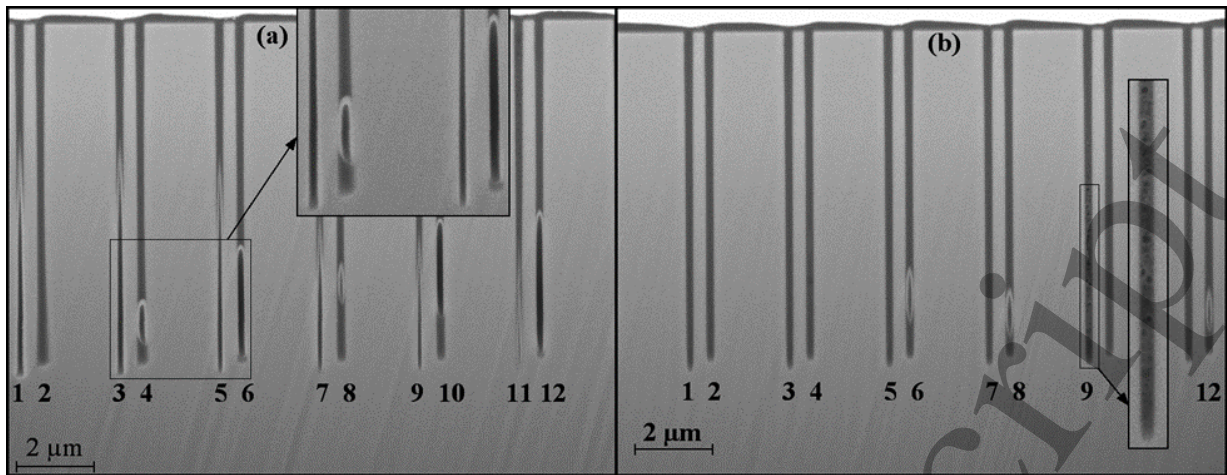


Figure 6. SEM images of the FIB cut in the DTI matrix showing the filling of the GKR 4602 in the trenches of sample 3 (without a pre-wetting layer). (a) Lack of photoresist and presence of large air bubbles; (b) Almost filled trenches with small air bubbles. The contrast and zooming in of images are modified using ImageJ software code [26].

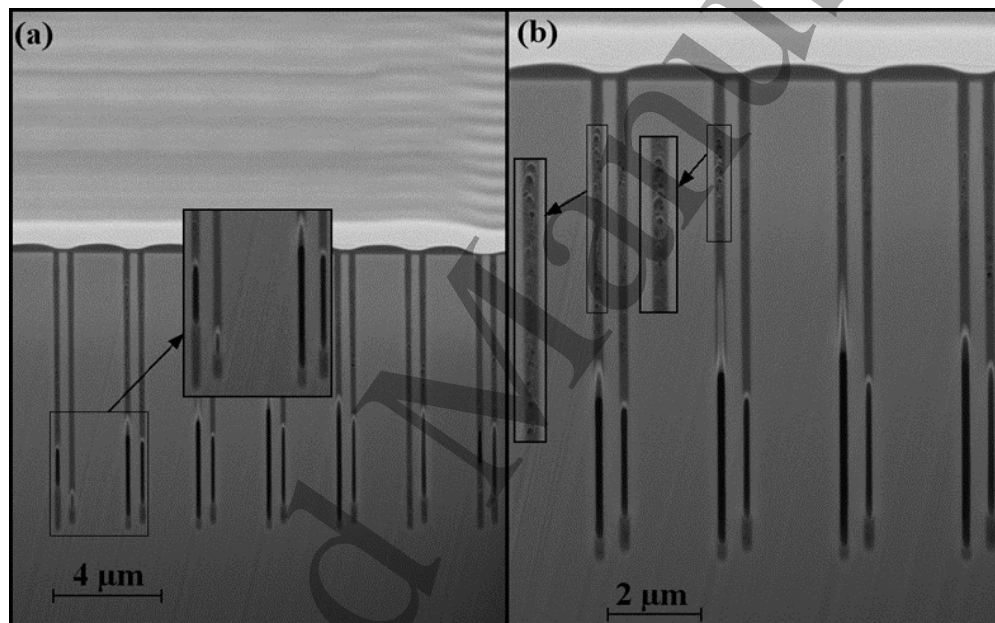


Figure 7. SEM images of the FIB cut in the DTI matrix showing the filling of the GKR 4602 in the trenches of sample 4 (with pre-wetting layer). (a) FIB cut on the DTI matrix; (b) Zoom on the FIB cut. The zooming in of images is modified using ImageJ software code [26].

bubbles (figure 6(a)) can be identified by the meniscus created by the photoresist [27]. In the second image (Figure 7(b)), although large air bubbles are present in all the trenches, the bottom of the trenches is actually filled with photoresist. Zooming in on Figure 7(b), small bubbles can be seen in the upper part of the trenches (small black holes), which could be explained by the fact that the bubbles could not escape from the trenches during the filling of the photoresist. These observations are in agreement with the conclusions obtained from the acoustic signal reading of sample 2, which showed a high wetting percentage and good wetting uniformity ($\bar{S}_2 = 92.3\%$, $\bar{\sigma}_2 = 5.9$).

The SEM images of the FIB cut indicate that we have a full wetting (100%) in the lower part of the trenches (see figure S3 in supplementary material). Furthermore, by observing the meniscus formed by the trapped bubbles, we notice the concave shape between the photoresist, when coated in the liquid state, the trapped air bubbles, and the trench walls. This concave shape indicates that the walls of the trenches are hydrophilic [28].

4. Conclusion

In this paper, we characterize the wetting behavior of the GKR 4602 photoresist on a DTI patterned wafer with an aspect ratio of 50. Using acoustic characterization, we showed that the use

of the PGEE pre-wetting layer (before coating the GKR 4602) increased the wetting percentage at the bottom surface of the trenches and also made it more uniform. This result was also confirmed using FIB-SEM imagery, which showed that the pre-treated sample revealed better filling at the bottom surface compared to the sample without it. In fact, this first layer, being a solvent, acted as a facilitator for the filling of the photoresist to the bottom surface of the trenches. However, in both cases (with and without the pre-wetting layer), we observed (Figure 6 and Figure 7) the presence of air bubbles suspended in the photoresist. The air bubbles ranged in size from very small bubbles to large gaps, creating discontinuities in the photoresist present in the trenches. These trapped bubbles were observed in previous work we conducted on DTI with an aspect ratio of 30 [29]: We showed that a transition to full wetting inside the trenches led to the release of bubbles. In the literature, we find several techniques to remove and control bubbles suspended in fluids, such as degassing the fluid and avoiding pressure drops in the dispense system [30], the addition of surfactants to lower the surface tension [31], or using megahertz acoustic waves to control the bubbles [32]. Some of these techniques could prove useful to eliminate the bubbles and are envisaged for future study. The combination of the acoustic method we developed and the FIB-SEM imagery has proven to be a powerful tool for understanding the wetting behavior of polymers on porous surfaces and could be used as a technique to study the uniformity of coated photoresists during lithography processes, for example. Although it is still a local investigative (conditioned by the surface area of the transducer and the length of the FIB cut) and destructive testing technique (etched by the FIB), it can provide a comprehensive view of the wetting process.

Supplementary materials

See supplementary materials for additional figures related to the DTI matrix and FIB cuts.

Authors declarations

Acknowledgments

We would like to acknowledge the two anonymous reviewers of this manuscript, whose attentive and thoughtful comments substantially improved the clarity and readability of this work.

This work was partially supported by the French Renatech network. This research work has been partially undertaken with the support of IEMN fabrication (CMNF).

The authors would like to thank the joint laboratory ST-IEMN and the NANO 2022 European project.

Conflict of interest

The authors have no conflicts to disclose.

Data availability

The data that support the findings of this study are available from the corresponding author upon reasonable request.

References

- [1] G. May, and C. Spanos, "Fundamentals of Semiconductor Manufacturing and Process Control," John Wiley & Sons, Inc: Hoboken, 2006, p. 1-24.
- [2] See: <https://www.clean-rooms.org/iso-cleanroom-standards/> for more information about cleanrooms classification; accessed 30 April 2023.
- [3] K. Sunju, Y. Chung, H. Seunghon, P. Jihoon, K. Ohun, P. Donguk, C. Sangjun, K. Seungwon, H. Kwonchul, and K. Won, "Chemical use in the semiconductor manufacturing industry," International Journal of Occupational and Environmental Health 24(3-4), 109-118 (2018).
- [4] S. Jihoon, "Chemical Mechanical Planarization-Related to Contaminants: Their Sources and Characteristics," in Emerging Contaminants, edited by A. Nuro (IntechOpen, London, 2021), pp. 1-17.
- [5] C. Chieh-Chun, W. Bing, and R. Srin, "Particle Deposition and Removal of Relevance to Wet Processing in Semiconductor Manufacturing," Particulate Science and Technology 33(5), 546-553 (2015).
- [6] Z. Lingqian, L. Yaoping, L. Zhihong, and W. Wei, "SF6 Optimized O2 Plasma Etching of Parylene C," Micromachines 9(4), 162 (2018).
- [7] J. Robin, P. Deepak, S. Moh, V. Soney, and A. Jamil, "Single layer thin photoresist soft etch mask for MEMS applications," Microsystem Technologies 24, 2277-2285 (2018).
- [8] M. Graef, "More Than Moore White Paper," 2021 IEEE International Roadmap for Devices and Systems Outbriefs, 1-47 (2021).
- [9] A. Yuya, Q. Le, and E. Sánchez, "Removal of Post Etch Residue on BEOL Low-K with Nanolift," Solid State Phenomena 314, 277-81 (2021).
- [10] A. Lallart, P. Garnier, E. Lorenceau, A. Cartellier, and E. Charlaix, "Cleaning surfaces from nanoparticles with polymer film: impact of the polymer stripping," Micro and Nano Engineering 1, 33-36 (2018).
- [11] N. Vrancken, J. Li, S. Sergeant, G. Vereecke, G. Doumen, F. Holsteyns, C. Chen, H. Terry, S. De Gendt, and X. Xu, "In-situ ATR-FTIR for dynamic analysis of superhydrophobic breakdown on nanostructured silicon surfaces," Scientific Reports 8, 11637 (2018).
- [12] A. Bard, and L. Faulkner, "Electrochemical Methods: Fundamentals and Applications, 2nd Edition," John Wiley & Sons, Inc: New York, 2001, p. 368-388.
- [13] A. Vieira, W. Cui, V. Jokinen, R. H. A. Ras, and Q. Zhou, "Through-drop imaging of moving contact lines and contact areas on opaque water-repellent surfaces," Soft Matter 19, 2350 (2023).
- [14] W. Xiao, C. Fu, C. Zhang, Z. Qiu, and B. Wang, "A Comprehensive Review of Wetting Transition Mechanism on the Surfaces of Microstructures from Theory and Testing Methods," Materials 15(14), 4747 (2022).
- [15] N. Yu, S. Kiani, M. Xu, and CC. Kim, "Brightness of Microtrench Superhydrophobic Surfaces and Visual Detection

- of Intermediate Wetting States,” *Langmuir* 37(3), 1206-1214 (2021).
- [16] C. Virgilio, J. Carlier, P. Campistron, M. Toubal, P. Garnier, L. Brousseau, V. Thomy, and B. Nongaillard, “Wetting Characterization of High Aspect Ratio Nanostructures by Gigahertz Acoustic Reflectometry,” *International Journal of Mechanical and Mechatronics Engineering* 10(3), 506-511(2016).
- [17] A. Salhab, J. Carlier, M. Toubal, P. Campistron, M. Neyens, B. Nongaillard, and V. Thomy, “Nanostructures wetting evaluation using ultra high frequency ultrasound,” *Proceedings SPIE 12002, Oxide-based Materials and Devices XIII 12002*, (2022).
- [18] K. Rykaczewski, T. Landin, M. Walker, J. Scott, and K. Varanasi, “Direct imaging of complex nano- to microscale interfaces involving solid, liquid, and gas phases,” *ACS Nano* 6(10), 9326-9334 (2012).
- [19] R. Dufour, P. Brunet, M. Harnois, R. Boukherroub, V. Thomy, and V. Senez, “Zipping effect on omniphobic surfaces for controlled deposition of minute amounts of fluid or colloids,” *Small* 8(8), 1229-1236 (2012).
- [20] A. Tournier, F. Leverd, L. Favennec, C. Perrot, L. Pinzelli, M. Gatefait, N. Cherault, D. Jeanjean, J.-P. Carrere, F. Hirigoyen, L. Grant, and F. Roy, “Pixel-to-Pixel isolation by Deep Trench technology: Application to CMOS Image Sensor,” *Proc. IISW, Hokkaido, JAPAN*, (2011).
- [21] G. Philippe, F. Dignat, and C. de Buttet, “Deep Trenches Cleanliness Challenges for CMOS Image Sensors,” *ECS Transactions* 80, 101-109 (2017).
- [22] C. Virgilio, Ph.D. thesis, Université de Valenciennes et du Hainaut-Cambresis, 2017.
- [23] Campistron, P., Carlier, J., Toubal, M., Dupont, L., Nassar, G., Nongaillard, B., Saad, N., & Gao, G., “High Frequency Ultrasound a Tool for Elastic Properties Measurement of Thin Films Fabricated on Silicon.”, *Trans Tech Publications*, 324, 277-281 (2011).
- [24] Li, Sizhe & Lamant, Sebastien & Carlier, Julien & Toubal, Malika & Campistron, Pierre & Xu, Xiumei & Vereecke, Guy & Senez, Vincent & Thomy, Vincent & Nongaillard, Bertrand, “High-Frequency Acoustic for Nanostructure Wetting Characterization.”, *Langmuir : the ACS journal of surfaces and colloids*, 30, 25, 7601–7608 (2014).
- [25] Dufour, Renaud & Saad, Nadine & Carlier, Julien & Campistron, Pierre & Nassar, Georges & Toubal, Malika & Boukherroub, Rabah & Senez, Vincent & Nongaillard, Bertrand & Thomy, Vincent, “Acoustic Tracking of Cassie to Wenzel Wetting Transitions.”, *Langmuir : the ACS journal of surfaces and colloids*, 29, 43, 13129–13134 (2013).
- [26] See:https://imagej.nih.gov/ij/macros/tools/Zoom_in_Images_and_Stacks.txt for information on the code used for Zoom in Images and Stacks macro tool; accessed 30 April 2023.
- [27] X. Gu, L. Shaw, K. Gu, M. Toney, and Z. Bao, “The meniscus-guided deposition of semiconducting polymers,” *Nature Communications* 9, 534 (2018).
- [28] F. Bunge, S. van den Driesche, M.J. Vellekoop, “Symmetric surficial phaseguides: a passive technology to generate wall-less channels by two-dimensional guiding elements,” *Microfluid Nanofluid* 20, 95 (2016).
- [29] A. Salhab, J. Carlier, M. Toubal, P. Campistron, M. Neyens, B. Nongaillard, and V. Thomy, “Analysis of Wetting Transition and Pattern Collapse During the Drying Process of Deep Trench Isolation Structures Using Ultra-high Frequency Acoustic Waves and SEM Imaging,” *Proceedings 16ème Congrès Français d'Acoustique, CFA2022, Société Française d'Acoustique, Marseille, France, April 2022*.
- [30] Aiwen Wu and Wailup Chow, "A technique for rapid elimination of microbubbles for photochemical filter startup", *Proc. SPIE 7140, Lithography Asia 2008, 71402Y* (2008).
- [31] Daisuke Kobayashi, Yoshiyuki Hayashida, Kazuki Sano, Koichi Terasaka, " Effect of surfactant addition on removal of microbubbles using ultrasound ", *Ultrasonics*, 54(6), 1425-1429 (2014).
- [32] Baresch, Diego and Valeria Garbin, “Acoustic trapping of microbubbles in complex environments and controlled payload release.” *Proceedings of the National Academy of Sciences of the United States of America* 117 (2020): 15490 – 15496.